Iraqi Journal of Physics, 2024
https://doi.org/10.30723/ijp.v22i3.1252
Vol. 22, No. 3, PP. 78-92
P-ISSN: 2070-4003
E-ISSN: 2664-5548

Current Density of $Al_xGa_{1-x}As/GaAs$ Superlattice

Ahmed Z. Obaid[1a], Nidhal M. Abdul-Ameer[1b]*, Shaymaa Q. Abdul-Hasan[1c], Ebtisam M-T. Salman[1d], and Moafak C. Abdulrida[2e]

[1] *Department of Physics, College of Education for Pure Science (Ibn Al-Haitham), University of Baghdad, Baghdad, Iraq*

[2] *Department of Medical Instrumentation Engineering Techniques Alsalam University College Baghdad, Iraq*

[a]*E-mail:ahmed.z.o@ihcoedu.uobaghdad.edu.iq*,[c]*E-mail: shaimaa.q.ah@ihcoedu.uobaghdad.edu.iq*
[d]*E-mail ibtisam.m.t@ihcoedu.uobaghdad.edu.iq*,[e]*E-mail: moafak.c.abdulrida@alsalam.edu.iq*
[b*]*Corresponding author: nidhal.m.aa@ihcoedu.uobaghdad.edu.iq*

Abstract

Theoretically, the $Al_xGa_{1-x}As/GaAs$ superlattice is studied as a function of optical energy with and without bias. The transfer matrix approach has determined the transmission coefficient and resonant tunnelling current density. The number of barriers is estimated at N = 3, and the concentration ratio (the mole fraction value) x at 0.1, 0.2, and 0.3 is fixed. The number of cells in the well is established at (ncw) = 5, while the number of barrier cells (ncb) is changed from 1 to 5 for both biases. This study shows that the change in the number of barrier cells plays a crucial role in the tunnelling of charge carriers and the transmission probability of charge carriers through the depletion regions. Thus, changing the current density is based on the purpose to be applied. In addition, the values of current density at the reverse bias are higher than that in the forward bias, which is explained by the bias controlling the energy levels of the superlattice. It is worth noting that there are many practical applications in which this system can be used, including solar cells, detectors, and light-emitting diodes.

Article Info.

Keywords:
Current Density, Resonant Tunnelling, $Al_xGa_{1-x}As/GaAs$ Superlattice, Transfer Matrix, Transmission.

Article history:
Received: Feb. 26, 2024
Revised: Jun. 15, 2024
Accepted: Jun. 21, 2024
Published: Sep. 01,2024

1. Introduction

Knowledge of semiconductor material properties with a good understanding of operational physical phenomena in device structures can lead to the successful design of any device in the semiconductor world [1-4]. Multiple potential barriers being crossed by the electron wave in resonant tunnelling is considered an important phenomenon in quantum mechanics [5]. The tunnelling transmission mechanism used in many quantum semiconductor devices allows for picosecond switching speeds. Due to resonant tunnelling, negative differential resistance can appear in these devices. The design of self-closing integrated logic circuits may be compatible with this characterization. On this basis, quantum hardware technology is an emerging and promising alternative to high-performance large-scale integration design [6]. One may consider the origin of the negative differential resistance mechanism whose associated instability leads to Electric Field Formation (EFD) in the Multi-Quantum Well (MQW) region. Semiconductor heterostructures, particularly double heterostructures such as quantum dots (QDs), quantum wires (QWRs), and quantum wells (QWs), have become a trending research topic for most of the semiconductor physics community [7]. The studied heterostructure consists of n-type $Al_xGa_{1-x}As$ and almost intrinsic or lightly doped p-type GaAs. It is one of the III-V compounds that is required to be a semiconducting material with unequal bandgaps to some extent, especially at small scales where the electronic

© 2024 The Author(s). Published by College of Science, University of Baghdad. This is an open-access article distributed under the terms of the Creative Commons Attribution 4.0 International License (https://creativecommons.org/licenses/by/4.0/).

properties depend on the spatial properties, especially those that depend on compounds [5]. The most prominent heterostructure of these compounds is GaAs/$Al_xGa_{1-x}As$ (or AlAs). Investigations into the physics and applications of semiconductor heterostructures have yielded tremendous advances since the initial theoretical proposals of Gubanov, Shockley and Cromer more than 50 years ago. The use of heterogeneous structures in the design and fabrication of semiconductor devices has led to significant improvements in performance that are achieved using current semiconductor device concepts [8] and led to the development of a wealth of new structures that could not have been achieved using simple homojunction technology. There are three important advantages of heterojunctions over homojunctions [9, 10]: 1) The cladding layer, for example, AlGaAs, has a larger bandgap than GaAs, so it will confine charge carriers to the central region where recombination is likely; this is known as carrier confinement, 2) Optical confinement is the process of forming an active region with a high refractive index that will act as an optical guide with observable optical focus as the efficiency of the stimulated emission increases, 3) because the laser emission process is only weak in nearby regions, losses are minimized. These three factors lead to a significantly lower threshold current density ($\sim 10^3$ A.cm^{-2}) than in the homojunction, enabling continuous wave operation at ambient temperature. Additionally, the AlGaAs/GaAs heterojunctions have band alignments that are staggered, which allows optical emission to be accomplished with photon energies significantly lower than the bandgap energies of both semiconductors constituting a heterojunction.

Reducing the thickness of the central active region is an important extension of the double-heterogeneous structure [11]. When the width of the well (10 nm in most III-V compounds) is less than a carrier's de Broglie wavelength in the well material, the carrier is "quantum" confined [12]. Due to its practical importance, many theoretical studies have been concerned with this field. A computational model has exhaustively explored the effect of the tunnelling electric field on resonant tunnelling across multibarrier systems of GaAs/$Al_yGa_{1-y}As$ using the transfer-matrix method [13]. A simplistic method was used by Talhi et al. to assess the photocurrent produced by $Al_xGa_{1-x}As$/GaAs solar cells [14]. Abolghasemi and Kohandani investigated the effects of strain on the electrical and optical characteristics of a p-i-n AlGaAs/InGaAs solar cell [15]. Panchadhyayee et al. presented an exhaustive study on tunnelling and electrical conduction in an electrically biased GaAs/$Al_yGa_{1-y}As$ generalised Fibonacci superlattice using transfer matrix formalism [16]. Vasilkova et al. studied the density of charge carrier distribution in AlGaAs/GaAs superlattices that were uniformly doped with layer thicknesses of 1.5/10 nm and different numbers of quantum wells [17].

In this work, resonant tunnelling through a one-dimensional multiple-barrier heterojunction superlattice structure of GaAs/AlGaAs was achieved. For this purpose, a theoretical model used the transfer matrix to compute the main parameters, such as the transmission coefficient and resonant tunnelling at forward and reverse biasing, which are very helpful in explaining the mechanism of the current density of the Al_xGa_{1-x} As/GaAs superlattice compared with different compositions.

2. Theoretical Part

2.1. GaAs/$Al_xGa_{1-x}As$ Superlattice Structure

GaAs/$Al_xGa_{1-x}As$ superlattices are constructed by growing two compounds characterized by almost identical lattice constants. Esaki [18] reported that for the symmetry of a superlattice model to resemble the Kronig–Penny model, there are two crucial requirements: (i) for materials with differing compositions, the energy mismatch at the band boundaries determines the height of the barrier, and (ii) the masses of the

carriers must differ in the well and barrier regions, in agreement with the effective masses at the edges of the conduction and valence bands, respectively. It would be better to consider a model to understand the tunnelling of electrons through a multibarrier semiconductor heterojunction. Therefore, such a model has a superlattice structure containing an alternating semiconductor heterojunction of $GaAs/Al_xGa_{1-x}As$. It should be noted that although these two materials' band structures are identical, their energy gaps differ. The GaAs have a small gap, and $Al_xGa_{1-x}As$ have a large energy gap. Due to the difference in the energy gaps, quantum barriers and quantum wells form, so GaAs forms the well, and $Al_xGa_{1-x}As$ forms the barrier. In this structure, the thickness of the barrier is (b), the thickness of the well is (a), and the superlattice period is (c) such that [c = a + b], as shown in Fig. 1.

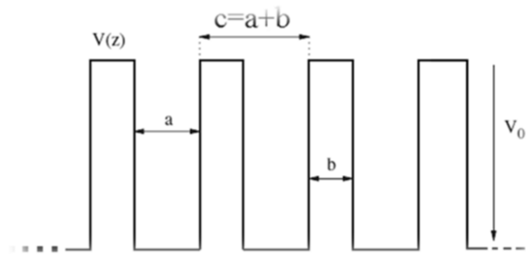

Figure 1: The periodic potential of a superlattice [5].

If the system consists of N barriers, one will find (N-1) wells, and N is estimated at N=3. A superlattice is formed with a periodic array of alternating layers of $GaAs/Al_xGa_{1-x}As$. The band gap difference between the two materials is considered to be equal to 88% of the barrier height (V_o) [19]:

$$V_o = 0.88(E_{gb} - E_{gw}) \quad (1)$$

where ($E_{gw} = 1.428$ eV) is the energy band gap in the well for (GaAs) and

$$E_{gb} = [1.428 + 1.247x]\text{eV} \quad (2)$$

E_{gb} is the barrier's energy band gap for $Al_xGa_{1-x}As$, as shown in Fig. 2.

Figure 2: Band alignment of ($GaAs/Al_xGa_{1-x}As$) in the direct-gap range.

The barrier height increases with the concentration of Al(x), where (x) is the composition or the value of the mole fraction [20]. The energy band gap of $Al_xGa_{1-x}As$ becomes indirect if (x) is greater than 0.45. So, x was considered at 0.1, 0.2, and 0.3 in

the present work. The well material's lattice constant (GaAs) is a_w=5.6533 Å [21], while the barrier material ($Al_xGa_{1-x}As$) is given by

a_b=[5.717x+ 5.686(1-x)]Å [lattice constant of $Al_xGa_{1-x}As$] **(3)**

It is well known that electrons behave dynamically as if their mass was the effect of the electron, m^*, instead of the mass of the electron, m_o in a vacuum. This observation is very important because the electron m^* is much smaller than m_o for many relevant semiconductors. For the junction of the GaAs/$Al_xGa_{1-x}As$ superlattice, the relationship between the Al content (x) and the effective masses is [22] $m_w^* = 0.065m_o$ and $m_b^* = (0.067 + 0.083x)m_o$, where m^* describes how a particle responds to a driving force; here, in the presence of the lattice, it is similar to a real mass [23].

2.2. Transfer Matrix of Al_xGa_{1-x} As / GaAs Superlattice

Energy levels in a quantum well structure can be determined by solving the Schrödinger equation for the wave function. The electron's potential energy V(z) according to the Ben Daniel-Duke equation of the description of the Schrödinger equation in one dimension with time independence is [13]:

$$\left[-\frac{\hbar^2}{2}\frac{d}{dz}\frac{1}{m^*}\frac{d}{dz} + V(z)\right]\psi(z) = \varepsilon\psi(z) \quad (4)$$

where (ε) is the energy of the bottom of the nth subbands, $(V(z))$ is the barrier potential:

$$V(z) = \begin{cases} V_o & \text{for } nc - \frac{b}{2} \leq z \leq nc + \frac{b}{2} \\ 0 & \text{otherwise} \end{cases} \quad (5)$$

Each region's wave function is calculated to solve an arbitrary structure's wave function [24]. The wave functions in the well region of the time-independent Schrödinger equation are expressed as follows:

$$\psi_n^{(w)}(z) = A_{2n-1}e^{ik_1 z} + B_{2n-1}e^{-ik_1 z} \quad (6)$$

where $k_1^2 = 2m_w^*\varepsilon/\hbar^2$, $n = 1, 2 \ldots, \mathcal{N}$, and $\mathcal{N}$ is the number of barriers.

It is possible to provide the barrier's region's wave function as [25]:

$$\psi_n^{(b)}(z) = \begin{cases} A_{2n}e^{-k_2 z} + B_{2n}e^{k_2 z} & \text{for} \varepsilon < V_o \\ A_{2n} + B_{2n}z & \text{for } \varepsilon = V_o \\ A_{2n}e^{ik_3 z} + B_{2n}e^{-ik_3 z} & \text{for } \varepsilon > V_o \end{cases} \quad (7)$$

where, $k_2^2 = 2m_b^*(V_o - \varepsilon)/\hbar^2$ and $k_3^2 = 2m_b^*(\varepsilon - V_o)/\hbar^2$. (k_2) and (k_3) are wave vectors; note that (k_2) becomes purely imaginary when $\varepsilon < V_o$. This case represents the situation inside the energy barrier, and the wave function becomes exponential without wave characteristics [26].

When employed at the nth barrier with the nth and $n+1^{th}$ area, the effective mass-dependent border provides requirements that preserve the probability [24, 26]:

$$\psi_n^{(w)}(z)\Big|_{nc-\frac{b}{2}} = \psi_n^{(b)}(z)\Big|_{nc-\frac{b}{2}}$$

$$\frac{1}{m_w^*}\frac{d\psi_n^{(w)}}{dz}\bigg|_{nc-\frac{b}{2}} = \frac{1}{m_b^*}\frac{d\psi_n^{(b)}}{dz}\bigg|_{nc-\frac{b}{2}} \tag{8}$$

$$\psi_n^{(b)}(z)\Big|_{nc+\frac{b}{2}} = \psi_{n+1}^{(w)}(z)\Big|_{nc+\frac{b}{2}}$$

$$\frac{1}{m_b^*}\frac{d\psi_n^{(b)}}{dz}\bigg|_{nc+\frac{b}{2}} = \frac{1}{m_w^*}\frac{d\psi_{n+1}^{(w)}}{dz}\bigg|_{nc+\frac{b}{2}} \tag{9}$$

where m_w^* and m_b^* are the effective masses in the well and barrier region, respectively. Through a series of surfaces and the space in between them, the matrix approach guides a ray. It can be determined that a 2×2 matrix multiplies the input values (y_0, θ_0) to produce the output values $(y_f\ , \theta_f)$. Matrix expressions for transformations include the following [6]:

$$\begin{bmatrix} y_2 \\ \theta_2 \end{bmatrix} = \begin{bmatrix} \mathcal{M}_{11} & \mathcal{M}_{12} \\ \mathcal{M}_{21} & \mathcal{M}_{22} \end{bmatrix} \begin{bmatrix} y_1 \\ \theta_1 \end{bmatrix}$$

where the matrix is noted by $\mathscr{M}$.

For the transformation matrix [5]:

$$\mathscr{M} = \begin{bmatrix} \mathcal{M}_{11} & \mathcal{M}_{12} \\ \mathcal{M}_{21} & \mathcal{M}_{22} \end{bmatrix} = \begin{bmatrix} \alpha & \beta \\ \gamma & \delta \end{bmatrix}$$

The ray transfer matrix shows the effects of an optical component on the ray. This matrix representation provides several surfaces and spaces with ray matrices: M_l; M_2; M_3; … M_N is shown by a single matrix that is the product of both of them [11, 27]:

$$\mathscr{M} = \mathcal{M}_N \cdots \mathcal{M}_3 \mathcal{M}_2 \mathcal{M}_1$$

The determinants follow the rule

$$\det\mathcal{M} = \det\mathcal{M}_N \cdots \det\mathcal{M}_3 \cdot \det\mathcal{M}_2 \cdot \det\mathcal{M}_1$$

2.3. Double-Quantum Well

The first potential barrier's initial coefficient of the electron wave is related to [13, 25]:

$$\begin{bmatrix} A_3 \\ B_3 \end{bmatrix} = \mathcal{M}_1 \begin{bmatrix} A_1 \\ B_1 \end{bmatrix} \tag{10}$$

where $\mathcal{M}_1$ is a 2×2 matrix (transfer matrix), which is related to the wave amplitude for waves at the right of the barrier (A_1, B_1) and the lift of the barrier (A_3, B_3), and it can be obtained by applying the wave function equations in boundary condition Eqs. (8) and (9):

$$\mathcal{M}_1 = \begin{bmatrix} \mathcal{M}_{11} & \mathcal{M}_{12} \\ \mathcal{M}_{21} & \mathcal{M}_{22} \end{bmatrix} \tag{11}$$

Substituting (11) in (10) gives

$$\begin{bmatrix} A_3 \\ B_3 \end{bmatrix} = \begin{bmatrix} \mathcal{M}_{11} & \mathcal{M}_{12} \\ \mathcal{M}_{21} & \mathcal{M}_{22} \end{bmatrix} \begin{bmatrix} A_1 \\ B_1 \end{bmatrix} \quad (12)$$

$$A_3 = \mathcal{M}_{11}A_1 + \mathcal{M}_{12}B_1$$

$$B_3 = \mathcal{M}_{21}A_1 + \mathcal{M}_{22}B_1 \quad (13)$$

$$(\mathcal{M}_1)_{11} = (\mathcal{M}_1)^*_{22}$$

$$(\mathcal{M}_1)_{12} = (\mathcal{M}_1)^*_{21}$$

$$\mathcal{M}_1 = \begin{vmatrix} \mathcal{M}_{11} & \mathcal{M}_{12} \\ \mathcal{M}^*_{21} & \mathcal{M}^*_{22} \end{vmatrix} \quad (14)$$

Here, the asterisk indicates the complex conjugate, where the matrix elements are [13, 25]:

$$(\mathcal{M}_1)_{11} = (\cosh k_2 b + \frac{k_2^2 f^2 - k_1^2}{2ik_1k_2f} \sinh k_2 b)e^{-ik_1b}$$

$$(\mathcal{M}_1)_{22} = \left(\cosh k_2 b + \frac{k_2^2 f^2 - k_1^2}{(-2ik_1k_2f)} \sinh k_2 b\right) e^{ik_1b} \quad (15)$$

$$(\mathcal{M}_1)_{12} = \frac{k_1^2 + k_2^2 f^2}{2ik_1k_2f} \sinh k_2 b$$

$$(\mathcal{M}_1)_{21} = \frac{k_1^2 + k_2^2 f^2}{(-2ik_1k_2f)} \sinh k_2 b \quad (16)$$

$f = \frac{m^*_w}{m^*_b}$ and yet $\mathcal{M}_1 = 1$.

2.4. Multi-Quantum Well

For multipotential barriers, the transfer matrix is related to the incident wave coefficient at the left of the MBS and the transmitted waves at the right of the MBS. Therefore, the left-hand wave's coefficient matrix of the nth barrier $\begin{bmatrix} A_{2n+1} \\ B_{2n+1} \end{bmatrix}$ and the right $\begin{bmatrix} A_{2n-1} \\ B_{2n-1} \end{bmatrix}$ appears as:

$$\mathcal{M}_n = (F^*)^{n-1}\mathcal{M}_1 F^{n-1} \quad (17)$$

where $F = \begin{bmatrix} e^{ik_1c} & 0 \\ 0 & e^{-ik_1c} \end{bmatrix}$ and n =1, 2… $\mathcal{N}$.

This approach can find a relation between the two coefficients A and B in the outmost layers [28, 29].

$$\begin{bmatrix} A_{2\mathcal{N}+1} \\ B_{2\mathcal{N}+1} \end{bmatrix} = \mathcal{M}_{\mathcal{N}}\mathcal{M}_{\mathcal{N}-1} \cdots \mathcal{M}_2\mathcal{M}_1 \begin{bmatrix} A_1 \\ B_1 \end{bmatrix} \quad (18)$$

The total barrier is [11, 13]:

$$\mathcal{W}_{\mathrm{n}} = \mathcal{M}_{\mathcal{N}}\mathcal{M}_{\mathcal{N}-1}\cdots\mathcal{M}_2\mathcal{M}_1$$

Substituting $(\mathcal{W}_{\mathrm{n}})$ in Eq. (18) gives:

$$\begin{bmatrix} A_{2\mathcal{N}+1} \\ B_{2\mathcal{N}+1} \end{bmatrix} = \mathcal{W}_{\mathrm{n}} \begin{bmatrix} A_1 \\ B_1 \end{bmatrix} \quad (19)$$

3. Transmission Coefficient

In a multibarrier system (MBS), the transmission coefficient can be defined as the relative probability that an incident electron may encounter multiple barriers. The transfer matrix method is used to derive the transmission coefficient [13]. Additionally, the transfer-matrix technique can be employed to determine a tunnel's inactive transmission coefficient (T) as a function of the energy incident upon it (ε) and the bias being used is (V) [30]:

$$\mathcal{W}_{\mathrm{n}} = (F^*)^{\mathcal{N}} G^{\mathcal{N}} \quad (20)$$

where the matrix $G = \mathcal{M}_1 F$.

$$G =$$

$$\begin{bmatrix} \left(\cosh k_2 b + \frac{k_2^2 f^2 - k_1^2}{2ik_1k_2f}\sinh k_2 b\right) e^{-ik_1b} e^{ik_1c} & \left(\frac{k_1^2 + k_2^2 f^2}{2ik_1k_2f}\sinh k_2 b\right) e^{-ik_1c} \\ \left(\frac{k_1^2 + k_2^2 f^2}{-2ik_1k_2f}\sinh k_2 b\right) e^{ik_1c} & \left(\cosh k_2 b + \frac{k_2^2 f^2 - k_1^2}{(-2ik_1k_2f)}\sinh k_2 b\right) e^{ik_1b} e^{-ik_1c} \end{bmatrix} \quad (21)$$

where $\mathcal{W}_{\mathrm{n}}$ is Hermitian and has a unit value for its determinant.

$$G_{tr} = G_{11} + G_{22}$$

where G_{tr} is a matrix trace G [31].

$$G_{tr} = \begin{cases} 2.\left[\cos k_1 a \,.\, \cosh k_2 b + \frac{k_2^2 f^2 - k_1^2}{2k_1k_2f} \,.\, \sin k_1 a \,.\, \sinh k_2 b\right] & \varepsilon < V_o \\ 2.\left[\cos k_1 a - \frac{k_1}{2f}\sin ka\right] & \varepsilon = V_o \\ 2.\left[\cos k_1 a \,.\, \cosh k_3 b - \frac{k_3^2 f^2 + k_1^2}{2k_1k_3f} \,.\, \sin k_1 a \,.\, \sinh k_3 b\right] & \varepsilon \geq V_o \end{cases} \quad (22)$$

The transmission coefficient (T), as a function of (ε, V), can be obtained across N barriers as follows:

$$T(\varepsilon, V) = \frac{|A_{2n+1}|^2}{|A_1|^2} \quad (23)$$

Since the multibarrier system's right end contains no reflected electrons, one can set $B_{2N+1} = 0$ [13, 32]. However, using this fact together with Eqs. (19) and (23), the transmission coefficient can be obtained as [13, 33]:

$$T(\varepsilon, V) = \frac{1}{|(W_N)_{11}|^2} = \frac{1}{1 + |(W_N)_{12}|^2} \tag{24}$$

$(W_N)_{12}$ can be obtained from

$$(W_N)_{12} = e^{-ik_1 Nc} G_{12} \frac{\lambda_2^N - \lambda_1^N}{\lambda_2 - \lambda_1} \tag{25}$$

$$|(W_N)_{12}|^2 = \begin{cases} |(M_1)_{12}|^2 \left|\frac{\sin N\theta}{\sin\theta}\right|^2 & G_{tr} < 2 \\ |(M_1)_{12}|^2 N^2 & G_{tr} = 2 \\ |(M_1)_{12}|^2 \left|\frac{\sinh N\theta}{\sinh\theta}\right|^2 & G_{tr} > 2 \end{cases} \tag{26}$$

4. Current Density

The current density through the structure of $Al_xGa_{1-x}As/GaAs$ is calculated using the Tsu-Esaki current formula [34]:

$$J(\varepsilon, V) = \frac{emK_BT}{2\pi\hbar^3} \int_0^\infty T(\varepsilon, V) \ln\left\{\frac{e^{\frac{(\varepsilon_f - \varepsilon)}{K_BT}} + 1}{e^{\frac{(\varepsilon_f - \varepsilon - eV)}{K_BT}} + 1}\right\} d\varepsilon \tag{27}$$

where K_B is Boltzmann's constant which is used to avoid any confusion with the wavevector k, ε_f is the Fermi level, V is the applied bias, and T is the room temperature.

5. Results and Discussion

In general, the transmittance of electrons through tunnelling depends on the electron energy. There are two effects on the probability of transmittance: the first is the thickness of the barrier through its superlattice number, where the probability decreases as the number of barriers increases. The second is the concentration ratio (x), where Fig. 3 and Fig. 4 show that the probability decreases with the increase in the concentration ratio as the thickness of the depletion region increases. It is noteworthy that tunnelling occurs at the energies of the infrared region with more energies than in the ultraviolet region because the interactions of electrons in the infrared region are of the type of vibrational interactions that require relatively little energy, while the electronic interactions in the ultraviolet region require high energy to occur. The tunnelling energies increase closer to each other by increasing the number of barriers at each concentration ratio due to the increase in the number of energy levels, where the probability of tunnelling for electrons is greater than if the number of energy levels is less. Where Eigen energies are often controlled consistently by the thickness of the outermost barrier in heterostructures, making them more applicable and effective for studying realistic systems [35].

It can be shown in Fig. 3, when forward bise; that electric tunneling is difficult as the barrier's width the number of barrier cells (nbc) increases. Additionally, more electrons suffer tunnelling at the same time. It has been observed that at lower

concentrations (0.1) (represented by the green colour), tunnelling has little effect on electrons, even when the barrier's width increases. Conversely, at higher concentrations (0.3), represented by the red colour, increasing the barrier's width affects electrons. The two protrusions in the curve just indicate the electrons' transit through the well. Because of the barrier separating the two wells, it is noted that the current reduces.

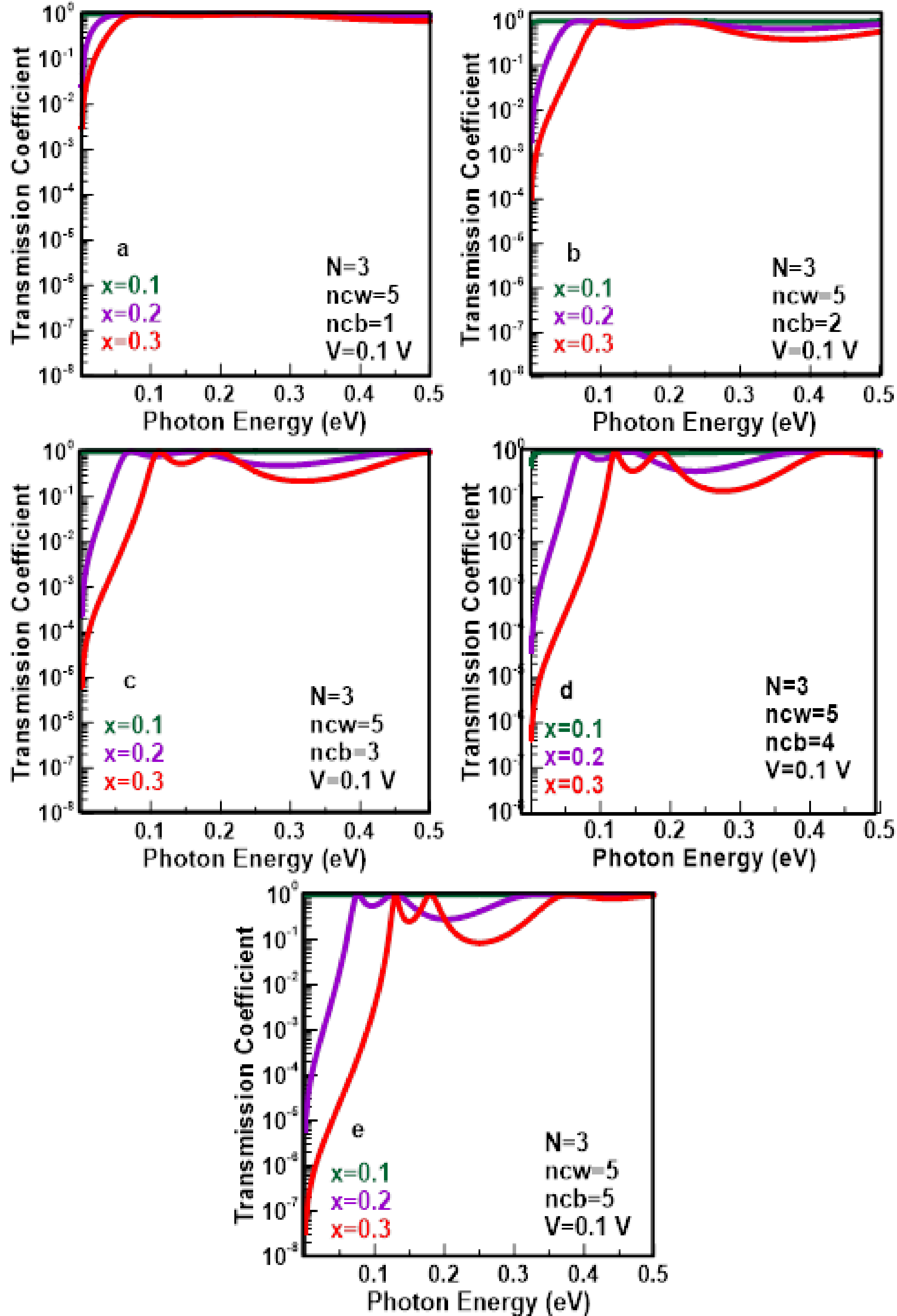

***Figure 3:** The transition coefficient of the $Al_xGa_{1-x}As/GaAs$ superlattice as a function of photon energy with (N=3), (ncw =5), and (from ncb=1 to 5) with forward basing (V=0.1 V) in a, b, c, d, e respectively. The concentration ratios are x=0.1 (green), x=0.2 (purple), and x=0.3 (red).*

For reverse catalysis, Fig. 4 depicts the same behaviour as Fig. 3, except for a blue energy shift. We think this is because reverse catalysis naturally widens the depletion region, which influences the energy of the electron that is expended. After all, this process needs electrons with higher energies than in forward bias. Where at forward bias tunnelling occurs for energies that take the range of the ultraviolet spectrum, while at reverse bias, tunnelling occurs close to the visible and infrared spectra. With this, it is possible to choose the appropriate energies for the application of the user. We observed strong agreement between our results and the reference [35].

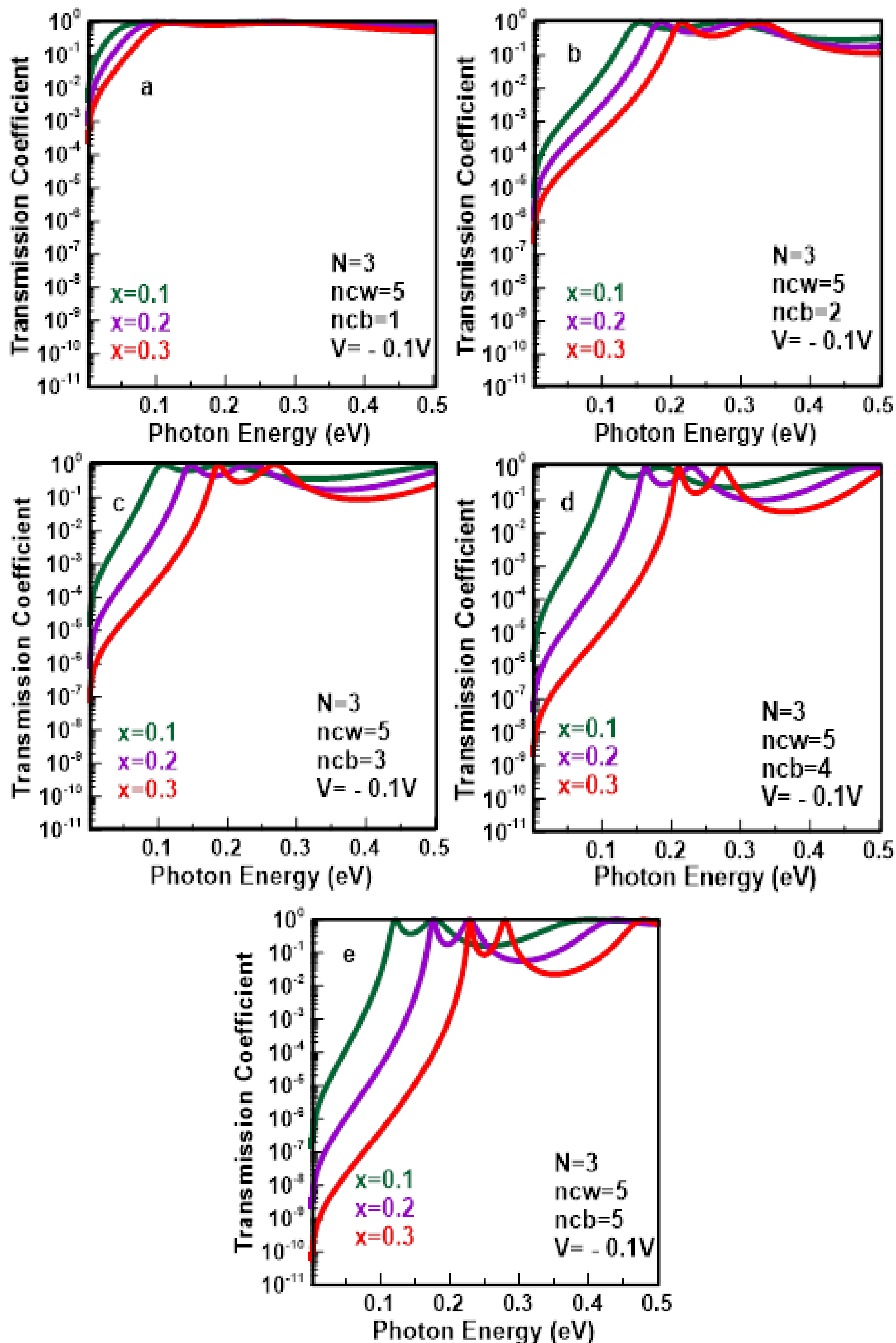

Figure 4: The transition coefficient of the $Al_xGa_{1-x}As/GaAs$ superlattice as a function of photon energy with (N=3), (ncw=5), and (from ncb=1 to 5) with the reverse basing (V=- 0.1 V) in a, b, c, d, e respectively. The concentration ratios are x=0.1 (green), x=0.2 (purple), and x=0.3 (red).

Fig. 5 shows the current density at the forward bias with a voltage of 0.1 V, where it is noted that the highest current values are at the energies of the infrared and visible regions, while they decrease in the ultraviolet region. As shown in Fig. 5, the current density level, which remains relatively high and takes a wide range of energies, is shown in Fig. 5d, where the number of cells (ncw) = 4, the concentration ratio = 0.2, and 0.1, this achieves the highest current density that can be achieved with the largest energy range of photons.

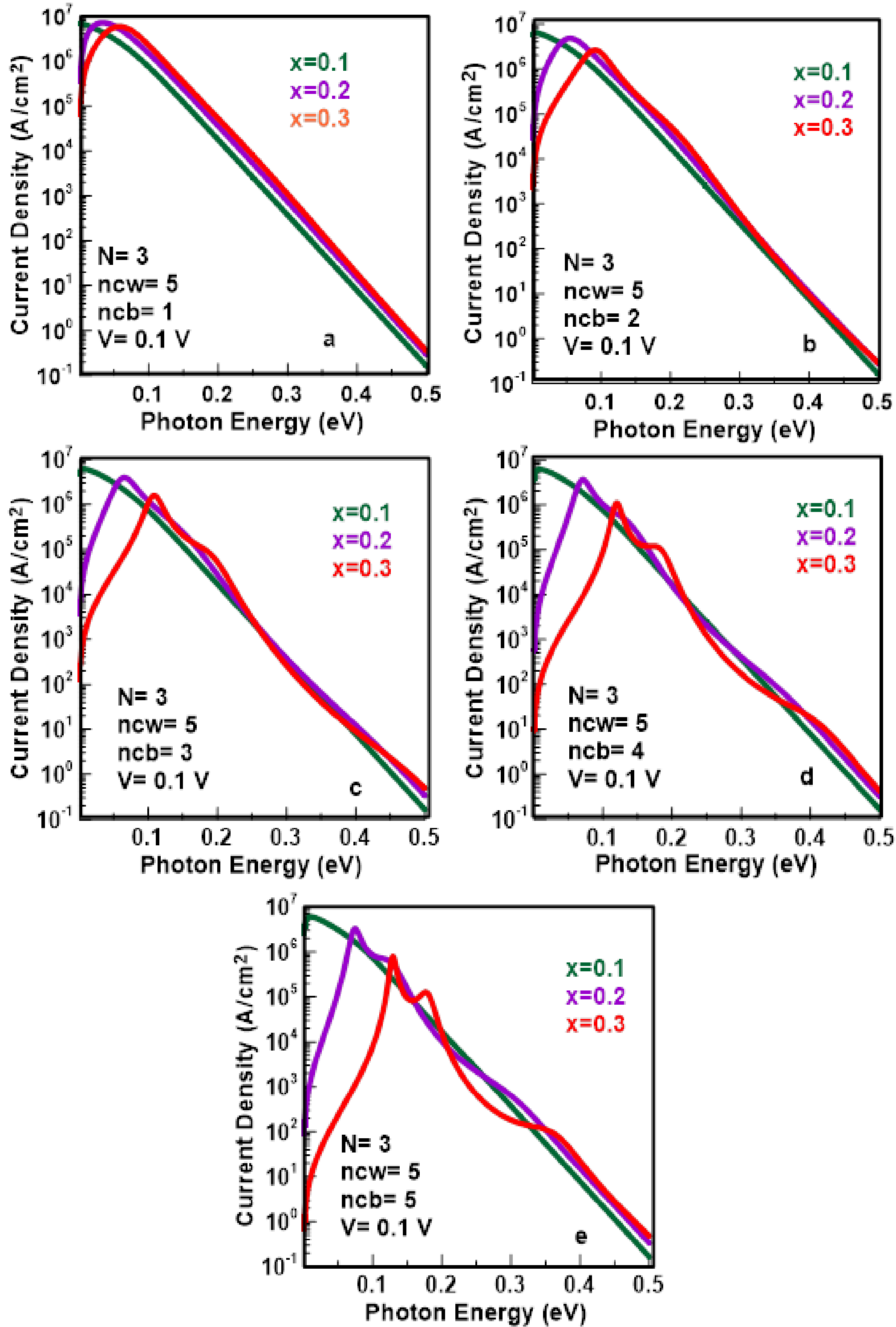

***Figure 5:** The current density of the $Al_xGa_{1-x}As$/ GaAs superlattice as a function of photon energy with (N=3), (ncw =5), and (from ncb = 1 to 5) with forward basing V=0.1 V in a, b,c,d,e respectively. The concentration ratios are x=0.1 (green), x=0.2 (purple), and x=0.3 (red).*

With an increase in concentration or the number of barrier cells, the stability of the current density will decrease, as there will be fluctuations in the rise and decrease of the current density. This is due to the occurrence of tunnelling for energies without others, as the current density increases at the largest energy range of photons.

In Fig. 6, which represents the current density, but in the reverse bias, where the applied bias is equal to -0.1 V, it is noted that a high current density value can be obtained and may be higher than it is in the forward bias whenever the number of barrier cells is less, which is logically reasonable. The barrier is thinner because the probability of electrons crossing over is greater. However, there is a different behaviour of the current at a concentration ratio of 0.3, where the highest current density is shown in Fig. 6a. Still, soon it starts decreasing faster than the rest of the current densities at concentration ratios of 0.2 and 0.1. The reason may be attributed to the fact that, under the conditions in Fig. 6a, a reverse current collapse occurred, which is the opposite of what was observed in the rest of the figures.

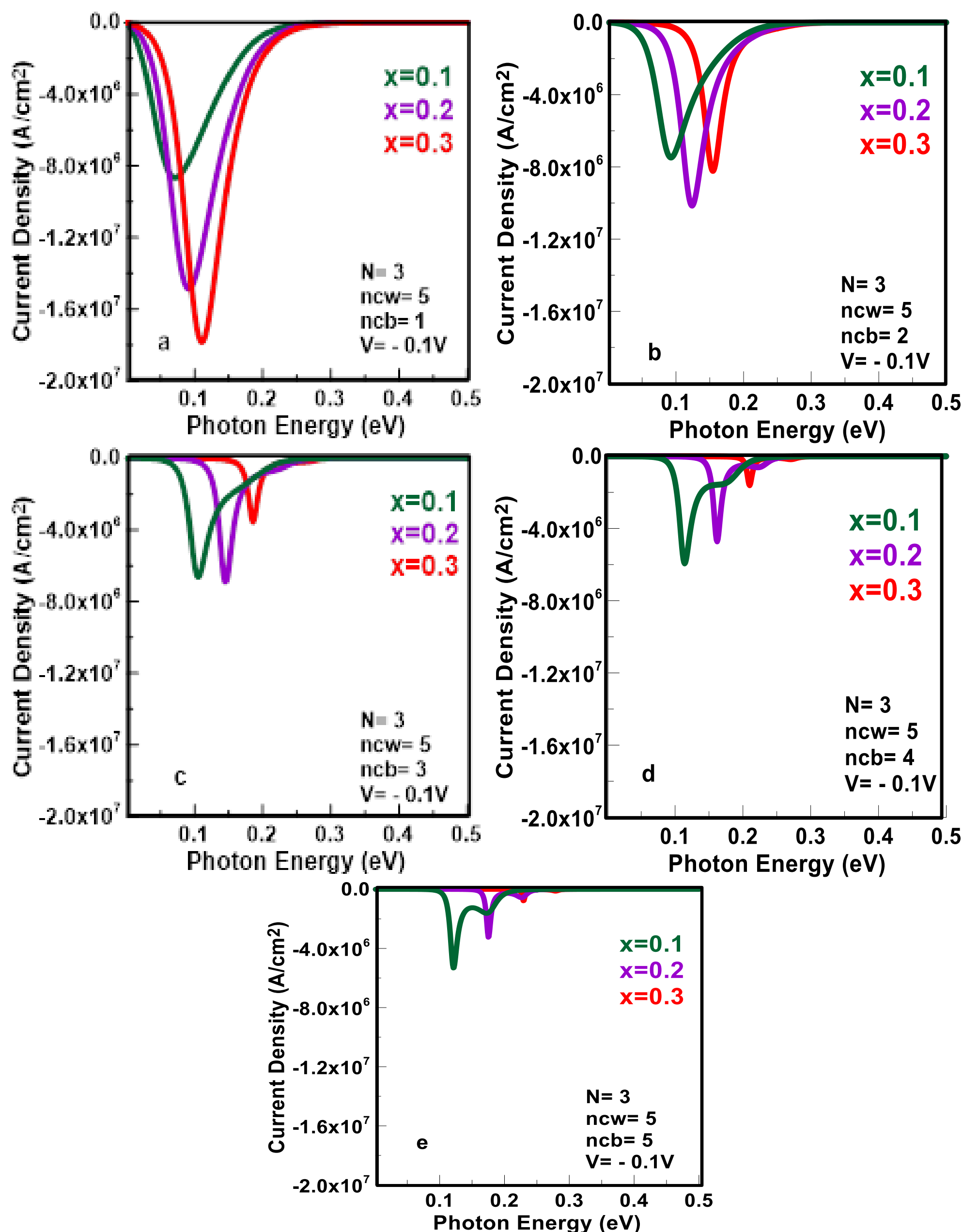

Figure 6: The current density of the $Al_xGa_{1-x}As$/ GaAs superlattice as a function of photon energy with (N=3), (ncw=5), and (from ncb= 1 to 5) with reserve basing (V=0.1 V) in a, b, c, d, e respectively. The concentration ratios are x=0.1 (green), x=0.2 (purple), and x=0.3 (red).

In Fig. 7, the solid curves represent the first energy level, while the discontinuous curves represent the ground energy level. It is noted that the energy levels increase at the reverse bias. In contrast, the values of the energy levels decrease at the forward bias, which confirms our interpretation of the increase in the current density with the reverse bias. Generally, it is noted that the energy levels at the reverse bias are higher than in the forward bias or no bias. The reason for this is that when the reverse bias is applied, an external field is created towards the original field [35], which leads to an increase in the voltage barrier, which leads to higher energy levels and vice versa for the energy levels at the forward bias.

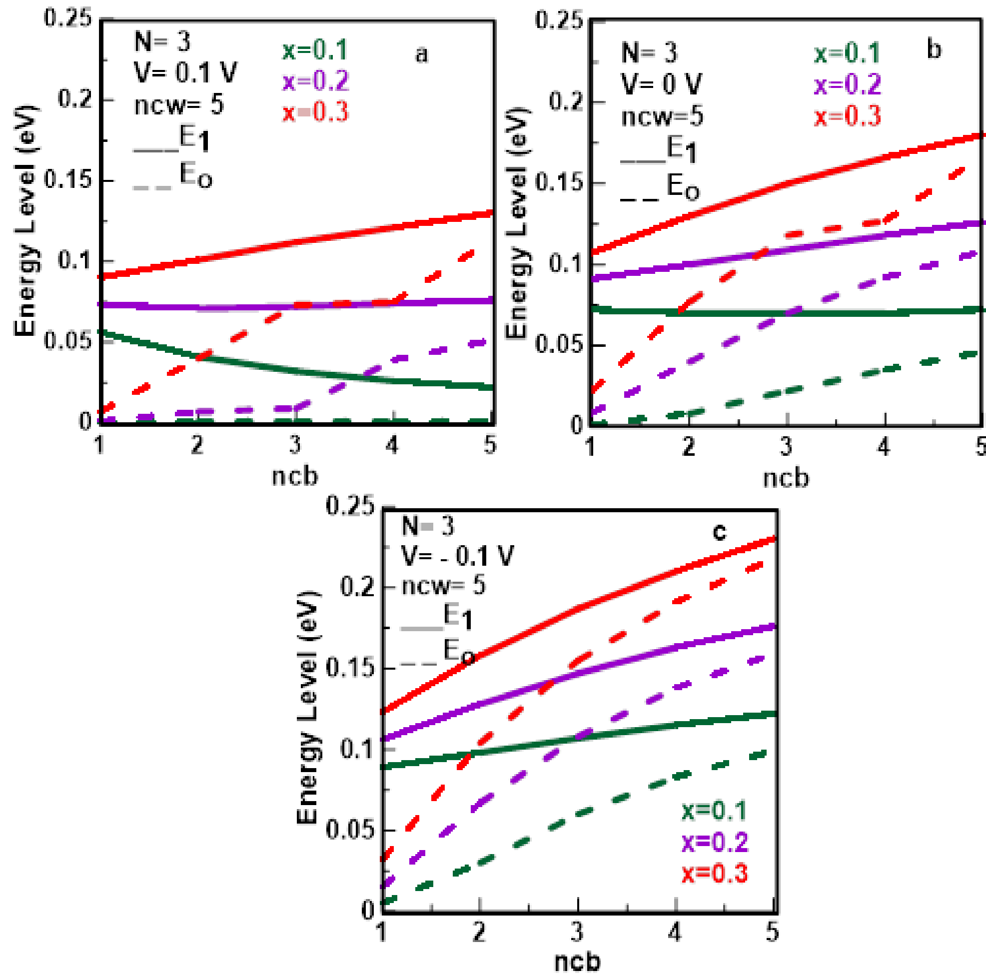

Figure 7: The Energy level of Al_xGa_{1-x} As/ GaAs Superlattice as a function of ncb with N=3 with the forward basing V=0, 1 V and the reverse basing V= - 0.1 V. The concentration ratios are x=0.1 (green), x=0.2 (purple), and x=0.3 (red).

6 .Conclusions

Several factors affect the transmission probability and the current density values in the formation of a superlattice, the most prominent of which in this study is the change in the width of the barrier (ncb). It is crucial to obtain the highest transmission probability of charge carriers by changing this factor, which is reflected in the values of the current density of the superlattice. A higher current density can be obtained at the reverse bias than the forward bias because the energy levels are higher due to the longer and more stable stay-lifetime of the electrons. Additionally, considering the energies at which tunnelling occurs and exploiting its position in the electromagnetic spectrum to be adopted by practical applications (solar cells, detectors, light-emitting diodes) can obtain the best results. In other words, there are energies of the electromagnetic

spectrum in which the probability of penetration is as high as possible, in contrast to the energies in which the probability falls.

Acknowledgement

The authors are grateful to Dr. Marwa N. Najemaldeen for contributing to this work through their careful scientific discussions.

Conflict of interest

Authors declare that they have no conflict of interest.

References

1. V. Kunets, Ph.D Thesis, Humboldt-Universität zu Berlin, Mathematisch-Naturwissenschaftliche Fakultät I, 2004.
2. M. R. Jobayr and E. M. T. Salman, Chinese J. Phys. **74**, 270 (2021). DOI: 10.1016/j.cjph.2021.07.041.
3. M. R. Jobayr and E. M. T. Salman, J. Semicond. **44**, 032001 (2023). DOI: 10.1088/1674-4926/44/3/032001.
4. M. R. Jubayr, E. M. T. Salman, and A. S. Kiteb, Ibn AL-Haitham J. Pure Appl. Sci. **23**, 95 (2010).
5. R. J. Martín-Palma, J. Martínez-Duart, and F. Agulló-Rueda, *Nanotechnology for Microelectronics and Optoelectronics* (Amsterdam, Netherlands, Elsevier, 2006).
6. P. Mazumder, S. Kulkarni, M. Bhattacharya, S. Jian Ping, and G. I. Haddad, Proce. IEEE **86**, 664 (1998). DOI: 10.1109/5.663544.
7. Z. I. Alferov, Chem. Phys. Chem. **2**, 500 (2001). DOI: 10.1002/1439-7641(20010917)2:8/9<500::AID-CPHC500>3.0.CO;2-X.
8. H. Kroemer, Proce. IEEE **70**, 13 (1982). DOI: 10.1109/PROC.1982.12226.
9. K. M. Qader and E. M. T. Salman, En. Proce. **157**, 75 (2019). DOI: 10.1016/j.egypro.2018.11.166.
10. E. Salmana, M. Jobayrb, and H. Hassuna, J. Ovon. Res. **18**, 617 (2022). DOI: 10.15251/JOR.2022.184.61.
11. F. G. Smith, T. A. King, and D. Wilkins, *Optics and Photonics: An Introduction* (England, John Wiley & Sons, 2007).
12. M. Semtsiv, Ph.D Thesis, Humboldt-Universität zu Berlin, Mathematisch-Naturwissenschaftliche Fakultät I, 2004.
13. J. Nanda, P. K. Mahapatra, and C. L. Roy, Phys. B Conden. Mat. **383**, 232 (2006). DOI: 10.1016/j.physb.2006.03.021.
14. A. Talhi, K. Bouzidi, A. Belghachi, and M. B. Azizi, Third International Conference on Energy, Materials, Applied Energetics and Pollution (Constantine,Algeria ICEMAEP, 2016). p. 574.
15. A. Abolghasemi and R. Kohandani, Appl. Opt. **57**, 7045 (2018). DOI: 10.1364/AO.57.007045.
16. P. Panchadhyayee, R. Biswas, A. Khan, and P. K. Mahapatra, J. Phys. Conden. Mat. **20**, 275243 (2008). DOI: 10.1088/0953-8984/20/27/275243.
17. E. I. Vasilkova, E. V. Pirogov, M. S. Sobolev, A. I. Baranov, A. S. Gudovskikh, R. A. Khabibullin, and A. D. Bouravleuv, Phys. Scrip. **99**, 025951 (2024). DOI: 10.1088/1402-4896/ad1cbb.
18. L. Esaki, IEEE J. Quant. Elect. **22**, 1611 (1986). DOI: 10.1109/JQE.1986.1073162.
19. D. Mukherji and B. R. Nag, Phys. Rev. B **12**, 4338 (1975). DOI: 10.1103/PhysRevB.12.4338.
20. J. W. Lee and M. A. Reed, J. Vacu. Sci. Tech. B Microelect. Proce. Phenom. **5**, 771 (1987). DOI: 10.1116/1.583745.
21. Y. Mao, X. X. Liang, G. J. Zhao, and T. L. Song, Journal of Physics: Conference Series (Prague, Czech Republic 2014). p. 012172.
22. W. L. Bloss, Phys. Rev. B **44**, 8035 (1991). DOI: 10.1103/PhysRevB.44.8035.
23. I. B. Spielman, Ph.D Thesis, California Institute of Technology, 2004.
24. P. Keshagupta, Sci. Tech. Asia **2**, 75 (2015).
25. C. Pacher, W. Boxleitner, and E. Gornik, Phys. Rev. B **71**, 125317 (2005). DOI: 10.1103/PhysRevB.71.125317.
26. M. Shen and W. Cao, Mat. Sci. Eng. B **103**, 122 (2003). DOI: 10.1016/S0921-5107(03)00159-4.
27. S. E. Lyshevski, *Nano and Molecular Electronics Handbook* (Boca Raton, CRC Press, 2018).
28. B. Jonsson and S. T. Eng, IEEE J. Quant. Elect. **26**, 2025 (1990). DOI: 10.1109/3.62122.
29. A. K. Ghatak, K. Thyagarajan, and M. R. Shenoy, IEEE J. Quant. Elect. **24**, 1524 (1988). DOI: 10.1109/3.7079.
30. S. S. Allen and S. L. Richardson, Phys. Rev. B **50**, 11693 (1994). DOI: 10.1103/PhysRevB.50.11693.

31. S. Shrestha, N. Bhusal, S. Byahut, and C. K. Sarkar, BIBECHANA **18**, 91 (2021). DOI: 10.3126/bibechana.v18i1.27450.
32. J. W. Choe, H. J. Hwang, A. G. U. Perera, S. G. Matsik, and M. H. Francombe, J. Appl. Phys. **79**, 7510 (1996). DOI: 10.1063/1.362422.
33. M. Vasconcelos, E. Albuquerque, and A. Mariz, J. Phys. Conden. Mat. **10**, 5839 (1998). DOI: 10.1088/0953-8984/10/26/012.
34. J. P. Sun, G. I. Haddad, P. Mazumder, and J. N. Schulman, Proce. IEEE **86**, 641 (1998). DOI: 10.1109/5.663541.
35. R. F. Jao and J. Z. Lai, Journal of Physics: Conference Series (IOP Publishing, 2023). p. 012039.

كثافة التيار للشبيكة الفائقة $Al_xGa_{1-x}As/GaAs$

أحمد زيد عبيد[1] و نضال موسى عبدالامير[1] وشيماء قاسم عبدالحسن[1] وابتسام محمد تقي سلمان[1] وموفق كاظم عبدالرضا[2]
[1]*قسم الفيزياء، كلية التربية للعلوم الصرفة / (ابن الهيثم)، جامعة بغداد*
[2]*قسم تقنيات هندسة الاجهزة الطبية كلية السلام الجامعه*

الخلاصة

تمت دراسة الشبكة الفائقة $Al_xGa_{1-x}As/GaAs$ من الناحية النظرية بوصفها دالة للطاقة البصرية مع وبدون انحياز. لقد حدد تقريب مصفوفة الانتقال كل من معامل الانتقال وكثافة تيار النفق الرنين. تم تثبيت عدد الحواجز وهو N=3 وكما ان نسبة التركيز (الكسر المولي) تم تثبيته حيث x=0.1, 0.2,0.3. تم حديد عدد الخلايا في البئر ncw=5, بينما كان يتراوح عدد الخلايا في الحاجز ما بين 1الى 5عند كلا الانحيازيين. برهنت هذه الدراسة على ان التغير في عدد خلايا الحاجز يلعب دورا مؤثرا في تنفيق حاملات الشحنة واحتمالية الانتقال لحاملات الشحنة عند منطقة الاستنزاف. لذا، فان التغيير في كثافة التيار يعتمد على الغرض المراد تطبيقه، إضافة الى ذلك فان قيم كثافة التيار عند الانحياز العكسي اعلى منها في التيار الامامي، وهو ما يفسره الانحياز الذي يتحكم في مستويات الطاقة في الشبكة الفائقة. من الجدير بالذكر ان هناك العديد من التطبيقات العملية التي يمكن استخدام هذا النظام فيها، بما في ذلك الخلايا الشمسية والكاشفات والصمامات الثنائية الباعثة للضوء.

الكلمات المفتاحية: كثافة التيار، التنفيق الرنيني، الشبيكة الفائقة $Al_xGa_{1-x}As$ / GaAs ،مصفوفة النقل، النقل.